Optics Letters

Octave-spanning coherent perfect absorption in a thin silicon film

Lorelle N. Pye, Massimo L. Villinger, Soroush Shabahang, Walker D. Larson, Lane Martin, and Ayman F. Abouraddy*

CREOL, The College of Optics & Photonics, University of Central Florida, Orlando, Florida 32816, USA
**Corresponding author: raddy@creol.ucf.edu*

Received 24 November 2016; revised 2 December 2016; accepted 2 December 2016; posted 2 December 2016 (Doc. ID 281422); published 23 December 2016

Although optical absorption is an intrinsic materials property, it can be manipulated through structural modification. Coherent perfect absorption increases absorption to 100% interferometrically but is typically realized only over narrow bandwidths using two laser beams with fixed phase relationship. We show that engineering a thin film's photonic environment severs the link between the *effective* absorption of the film and its *intrinsic* absorption while eliminating, in principle, bandwidth restrictions. Employing thin aperiodic dielectric mirrors, we demonstrate coherent perfect absorption in a 2 μm thick film of polycrystalline silicon using a single *incoherent* beam of light at all the resonances across a spectrally flat, octave-spanning near-infrared spectrum, ≈800–1600 nm. Critically, these mirrors have wavelength-dependent reflectivity devised to counterbalance the decline in silicon's intrinsic absorption at long wavelengths.

OCIS codes: (230.4040) Mirrors; (260.3160) Interference; (230.4170) Multilayers.

https://doi.org/10.1364/OL.42.000151

The burgeoning study of non-Hermitian photonic structures is enabling new capabilities by sculpting the spatial distribution of the imaginary component of the refractive index, whether loss [1,2] or gain [3,4]. For example, interference can help *increase* absorption in low-loss materials—so-called "coherent perfect absorption (CPA)" [5–7]. The CPA concept is related to "critical coupling" [8,9], well known in microwave engineering [10], where light coupled to a cavity is strongly absorbed on resonance. CPA is now envisioned to facilitate a host of novel optical switching phenomena [11–13] as a means for strong coupling to two-dimensional materials [14,15], and has even been extended to acoustics [16]. To date, however, CPA has been realized at resonances lying within narrow bandwidths using two laser beams with a fixed phase relationship (a 3 nm bandwidth in a 100 μm thick Si film by tuning a continuous-wave laser [6]) or at single wavelengths in plasmonics- [17,18] and metamaterials-based [19] realizations. While proposals to increase the CPA bandwidth have been put forth [20,21], experimental realizations have not been forthcoming.

Our goal here is to address the following challenge: can one arrange for the *effective* absorption of a material, without modifying the material itself, to be controllably enhanced beyond its *intrinsic* absorption over a broad spectrum? In this Letter, we sever the link between the effective absorption of a structure and its intrinsic material absorption by sculpting the materials photonic environment. Specifically, we embed a 2 μm thick polycrystalline Si film in a planar resonator composed of rising *aperiodic*, multilayer dielectric mirrors and demonstrate spectrally flat CPA *on resonance* across an octave of bandwidth in the near-infrared (NIR), 800–1600 nm. The central insight for increasing the CPA bandwidth is that the decline in Si absorption at longer wavelengths necessitates the use of cavity mirrors whose reflectivity *amplitude* increases in-step with the wavelength. This Letter introduces decisive advances, in addition to the record CPA bandwidth achieved. We use a *single-beam* configuration in optimized symmetric and asymmetric structures to *match* or *exceed* the total absorption in two-beam CPA [22]. This approach thus also facilitates utilizing *in*coherent, rather than coherent, light, thereby expanding the scope of potential applications.

We first highlight a fundamental feature concerning absorption in planar photonic structures. If the absorption upon "one-sided-incidence" on a *symmetric* structure is $\mathcal{A}_1$ [Fig. 1(a)], then the absorption in a "two-sided-incidence" configuration [Fig. 1(b)] for the *same* structure is $\mathcal{A}_2 = \mathcal{A}_1 - 4\mathrm{Re}\{t_L^* r_L\}|a||b|\cos\phi$; ϕ is the relative phase between the incident field amplitudes a and b, $|a|^2 + |b|^2 = 1$, and r_L and t_L are the field reflection and transmission coefficients, respectively. Interference in this linear system may therefore raise $\mathcal{A}_2$ above $\mathcal{A}_1$, potentially to 100%, or lower it to 0% [22]. Although the interference term $\mathrm{Re}\{t_L^* r_L\}$ is zero in any lossless planar symmetric structure (the reflected and transmitted fields are in quadrature and thus cannot interfere [23]), it can become non-zero in non-Hermitian structures; i.e., introducing loss *enables* such interference. Maximizing this absorption-mediated interference requires (1) $|a| = |b|$ and $\phi = 0$ or π; and (2) a structure characterized by $|r_L| = |t_L|$ and a relative phase $\theta = 0$ or π between the reflection and transmission coefficients. If these conditions are satisfied at a given wavelength, then CPA ($\mathcal{A}_2 = 1$) is achieved, provided that $\cos\phi\cos\theta = -1$ [22]. This phenomenon has its origin in the emergence of a "dark state: a zero eigenvalue of the system's scattering matrix" whose corresponding

eigenvector dictates the relative amplitude and the phase of the incident fields to undergo CPA [5]. In *asymmetric* structures [Fig. 1(c)] provided with a back reflector ($t_L = 0$), the one-sided absorption $\mathcal{A}_1^a = 1 - |r_L|^2$ reaches 100% when $r_L = 0$. (The superscript "a" hereon refers to asymmetric structures.)

The specific architecture we consider consists of a Si film placed between two lossless mirrors M_1 and M_2 to form a symmetric Fabry–Perot resonator [Figs. 1(d) and 1(e)], or a back reflector M_2^a and a "front mirror" M_1^a that form an asymmetric resonator [Fig. 1(f)]. If the complex refractive index of Si is $n_{Si} = n + in'$, then the single-pass (or *intrinsic*) absorption in a layer of thickness d is $\mathcal{A} = 1 - e^{-2k'd}$, where $k' = n'\frac{2\pi}{\lambda}$ and λ is the free-space wavelength. The effective absorption in the Si film is *not* necessarily maximized by placing it between mirrors with high reflectivity. Instead, $\mathcal{A}$ determines the optimal values of mirror reflectivities that maximize $\mathcal{A}_1$, $\mathcal{A}_2$, or $\mathcal{A}_1^a$ by striking a balance between interference and absorption. For one-sided incidence in a symmetric structure, taking the reflectivities of M_1 and M_2 to be $R = R_1 = (2 - 3\mathcal{A})/\{(1 - \mathcal{A})(2 + \mathcal{A})\}$ optimizes $\mathcal{A}_1 = 0.5\cosh^2 k'd \geq 0.5$ [Fig. 2(a)]; i.e., a minimum of 50% absorption is achieved on resonance *independently* of $\mathcal{A}$ in the range $0 < \mathcal{A} \leq \frac{2}{3}$, at the end of which $\mathcal{A}_1 = \mathcal{A} = \frac{2}{3}$. On the other hand, two-sided incidence on a symmetric structure with mirrors having $R = R_2 = 1 - \mathcal{A}$ [Fig. 2(a)] yields $\mathcal{A}_2 = 1$ when the appropriate relative amplitude and phase are selected for the incident fields. For low $\mathcal{A}$, $R_1 \approx R_2$: the same mirrors optimize one- *and* two-sided absorption in a low-loss film placed in a symmetric structure [Fig. 2(a)]. In the asymmetric structure, it can be shown that choosing $R_1^a = (1 - \mathcal{A})^2$ for the *front* mirror M_1^a eliminates reflection altogether, $r_L = 0$, and results in perfect one-sided absorption $\mathcal{A}_1^a = 1$ (note that $R_1^a \leq R_2$).

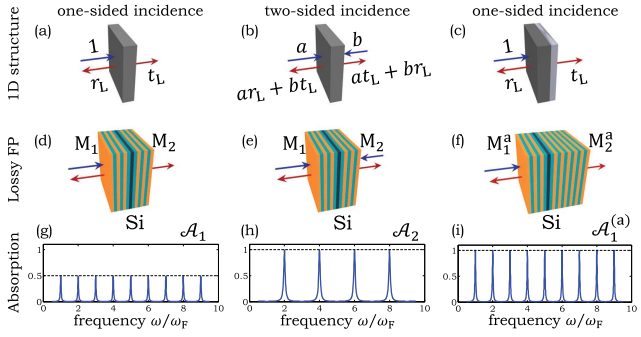

Fig. 1. Coherent absorption in a planar structure. (a) One-sided incidence on a generic structure; r_L and t_L are the field reflection and transmission coefficients for left incidence. One-sided absorption is $\mathcal{A}_1 = 1 - |r_L|^2 - |t_L|^2$. (b) Two-sided incidence on a symmetric structure. Two-sided absorption is $\mathcal{A}_2 = 1 - |ar_L + bt_L|^2 - |br_L + at_L|^2$. (c) One-sided incidence on an asymmetric planar structure with a back reflector ($t_L = 0$). One-sided absorption is $\mathcal{A}_1^a = 1 - |r_L|^2$. (d) One- and (e) two-sided incidence on a symmetric cavity consisting of a thin film of Si between multilayer mirrors M_1 and M_2. (f) One-sided incidence on an asymmetric cavity consisting of a thin film of Si between mirrors M_1^a and M_2^a. (g) $\mathcal{A}_1(\lambda)$ for the symmetric device in (d) with ideal mirrors; $\mathcal{A}_1 = 0.5$ at all the resonances; ω is the frequency, and ω_F is the free spectral range. (h) $\mathcal{A}_2(\lambda)$ for the symmetric device in (e) with ideal mirrors; $\mathcal{A}_2 = 1$ at only half the resonances, and $\mathcal{A}_2 = 0$ at the other half. The two incident fields are equal in amplitude and have a fixed phase relationship. (i) $\mathcal{A}_1^a = 1$ at all the resonances for the asymmetric device in (f) with an ideal front mirror M_1^a and a unity-reflection back mirror M_2^a.

Although the optimal one-sided absorption $\mathcal{A}_1 \geq 0.5$ occurs at all the resonances [Fig. 1(g)], the optimal two-sided absorption is achieved at only half the resonances since $\mathcal{A}_2 = 1 - \frac{1}{2}\{1 - (-1)^m \cos\phi\}\mathrm{sech}^2 k'd$, where m is the resonance order [Fig. 1(h)]. If $\phi = 0$ ($\phi = \pi$); even-ordered (odd-ordered) resonances undergo complete absorption. Therefore, when a broad bandwidth is of interest, the simpler and more stable one-sided incidence, surprisingly, yields a *larger* total absorption than optimal two-sided CPA, with no need to arrange for beam interference. Critically, the optimal asymmetric configuration provides the best performance with complete absorption at all the resonances, thus yielding *twice* the absorption of two-sided CPA [Fig. 1(i)].

We have therefore established that the reflectivity of M_1 or M_1^a required for maximal absorption is predicated on the intrinsic absorption $\mathcal{A}$. Since all materials have wavelength-dependent $\mathcal{A}$, achieving $\mathcal{A}_2 = 1$ and $\mathcal{A}_1 \geq 0.5$ in a symmetric structure, or $\mathcal{A}_1^a = 1$ in an asymmetric structure, over a large enough bandwidth, whereupon $\mathcal{A}$ varies substantially, therefore necessitates the use of mirrors *whose spectral reflectivity also changes with a wavelength* to counterbalance the spectral variation in $\mathcal{A}$. Consequently, Bragg or other mirrors with flat spectral reflectivity are optimal in only a limited wavelength span. The measured $\mathcal{A}(\lambda)$ for a 2 μm thick layer of polycrystalline Si is shown in Fig. 2(b). By combining this measured $\mathcal{A}(\lambda)$ with the theoretical optimal reflectivity [Fig. 2(a)], we obtain the target spectral reflectivities $R_1(\lambda)$ and $R_2(\lambda)$ that maximize

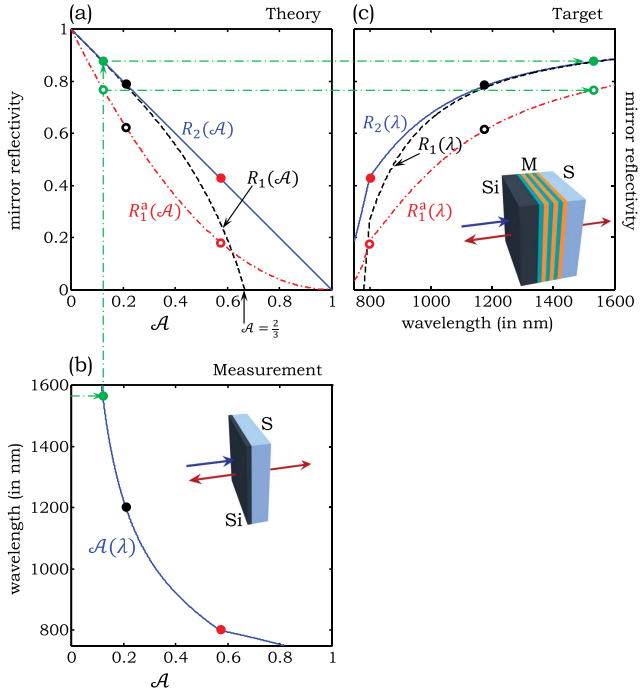

Fig. 2. Optimal mirror reflectivity for CPA. (a) R_1 and R_2 in a symmetric cavity for optimal one- and two-sided absorption $\mathcal{A}_1$ [Fig. 1(d)] and $\mathcal{A}_2$ [Fig. 1(e)], respectively, and R_1^a for optimal one-sided absorption $\mathcal{A}_1^a$ in an asymmetric cavity [Fig. 1(f)]–all versus $\mathcal{A}$. (b) Measured $\mathcal{A}$ in a 2 μm thick layer of poly-Si on a glass substrate (S). The plot is rotated to align the $\mathcal{A}$-axes in (a) and (b). (c) Target $R_1(\lambda)$, $R_2(\lambda)$, and $R_1^a(\lambda)$ to optimize $\mathcal{A}_1$, $\mathcal{A}_2$, and $\mathcal{A}_1^a$, respectively. Insets show schematic configurations. Three equally spaced wavelengths are selected in (b), and the dashed-dotted arrows trace the transformation from measured absorption to target mirror reflectivity.

$\mathcal{A}_1(\lambda)$ and $\mathcal{A}_2(\lambda)$, respectively, and $R_1^a(\lambda)$ that maximizes $\mathcal{A}_1^a(\lambda)$ [Fig. 2(c)]. The decline in Si NIR absorption requires that R increases with λ in all cases.

We carried out the inverse design of the target mirror in the symmetric device $R_2(\lambda) = 1 - \mathcal{A}(\lambda)$ [Fig. 2(c)] to optimize two-sided absorption using the FilmStar software package (FTG Software Associates) that employs damped least-squares optimization to synthesize the structure at each target reflectivity point [24]; $R_2(\lambda)$ simultaneously optimizes one-sided absorption for low $\mathcal{A}$ [Fig. 2(a)]. Using lossless materials with indices $n_L = 1.5$ and $n_H = 2.45$, we optimized the structure design iteratively to reduce the number of layers N to $N = 13$ for M_1 and M_2 in a symmetric structure. The resulting mirror has a reflectivity that approaches the target over an octave of bandwidth ~800–1600 nm in the NIR [Fig. 3(a)]. The mirror thickness is ≈2.2 μm, resulting in a total device thickness of $\approx 2 \times 2.2 + 2 = 6.4$ μm. For asymmetric configurations, we design a mirror M_1^a having reflectivity $R_1^a = [1 - \mathcal{A}(\lambda)]^2$ [Fig. 3(c)] and a back reflector M_2^a having flat unity-reflectivity over the bandwidth octave of interest [Fig. 3(e)]. In this design, M_1^a (M_2^a) consists of 14 (30) alternating layers of total thickness of 1.8 μm (4.5 μm). The total asymmetric device thickness is 8.3 μm. Note that the mirror thicknesses in both devices are on the order of that of the Si layer, and they may be further reduced using high-index-contrast materials [25]. Increasing N (a thicker device) enables more accurate approximation of the desired target spectral reflectivity $R(\lambda)$. In general, we find that errors in $R(\lambda)$ almost always result in a reduction of absorption.

The full symmetric device structure ($M_1 + Si + M_2$) was fabricated sequentially using physical vapor deposition employing the dielectrics ZnSe ($n_H = 2.45$) and ThF_4 ($n_L = 1.5$); other dielectric pairs may of course be employed instead. First, alternating ZnSe and ThF_4 layers are deposited from resistive targets on BK7 substrates (refractive index $n_s = 1.52$) to form M_1; a 2 μm thick polycrystalline Si layer is added via e-beam evaporation; finally, M_2 is deposited with the reverse layer-order of M_1. With the addition of a 1 mm thick borosilicate glass slide after M_2, we obtain a symmetric structure. The measured spectral reflection from M_1 is shown in Fig. 3(b) compared to a transfer-matrix calculation. Note that incidence is from air in Fig. 3(b), and not from Si as in Fig. 3(a), which dramatically changes the spectral reflection from this mirror. The asymmetric device $M_1^a + Si + M_2^a$ was similarly fabricated and characterized. Mirror M_1^a was designed, assuming incidence from air, and no extra glass slide is required here. Measurements for M_1^a and M_2^a are presented in Figs. 3(d) and 3(f), respectively.

We now proceed to the optical characterization of the complete symmetric device in the one-sided-incidence configuration [Figs. 4(a) and 4(b)], carried out using the setup in Fig. 4(c) for normally incident light. In contrast to reported CPA measurements, our measurements have been performed with incoherent light: a collimated beam from a Tungsten lamp. We measure the transmission T_L and reflection R_L coefficients, from which we determine $\mathcal{A}_1 = 1 - R_L - T_L$ [Figs. 4(g)–4(i)], $R_L = |r_L|^2$ and $T_L = |t_L|^2$, and compare the measurements to calculated values [Figs. 4(d)–4(f)]. The spectral phase $\alpha(\lambda)$ of reflection from M_1 and the refractive index of Si $n(\lambda)$ determine the locations of the resonances through $\alpha(\lambda) + n(\lambda)\frac{2\pi}{\lambda}d = m\pi$

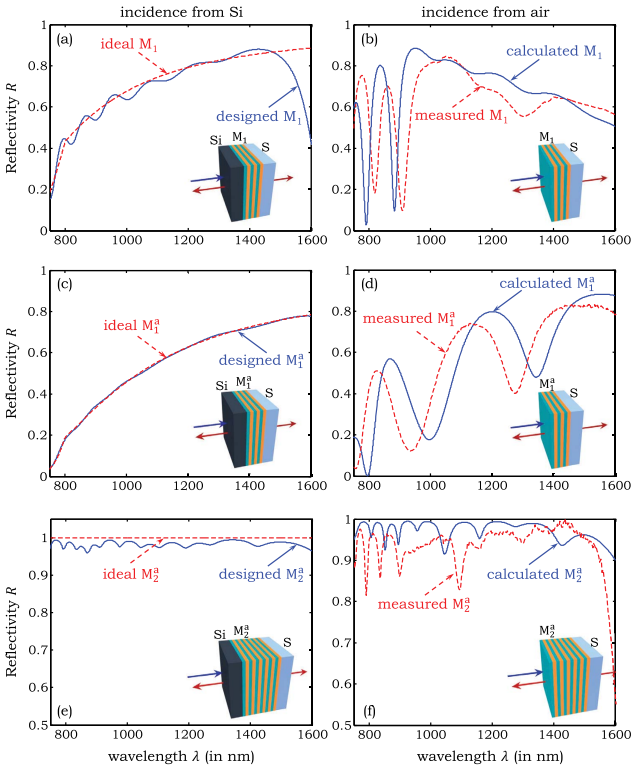

Fig. 3. Mirror design for CPA. (a) Calculated spectral reflectivity of the design mirror M_1 for the symmetric device on a glass substrate S (solid curve), compared to the target reflectivity (dashed curve) from Fig. 2(a) when incidence is from Si. (b) Calculated (solid curve) and *measured* (dashed curve) reflectivity of the fabricated mirror M_1 on a glass substrate S when incidence is from air. (c) and (d) Same as (a) and (b) for the front mirror M_1^a of the asymmetric device. The curves in (c) coincide closely with each other. (e) and (f) Same as a and b for the back reflector M_2^a of the asymmetric device (note the reduced vertical scale).

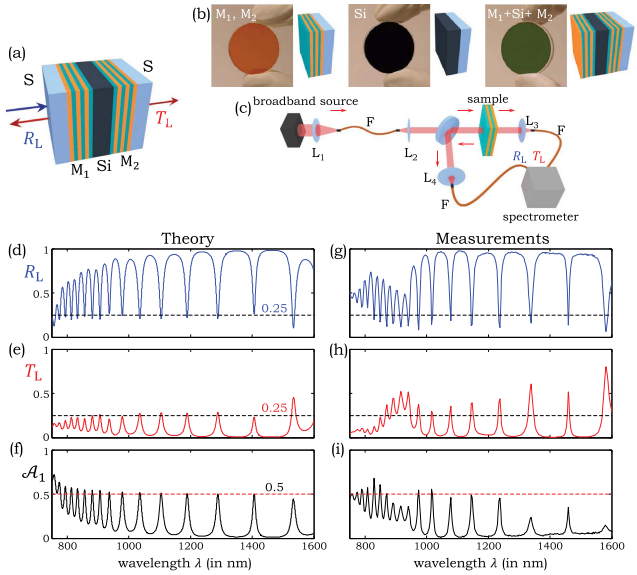

Fig. 4. One-sided absorption in a symmetric cavity. (a) Schematic of the device; S, substrate. (b) Photographs of 25 mm diameter samples: mirror M_1, thin Si film (2 μm thick), and the device $M_1 + Si + M_2$, all on BK7 substrates. (c) Schematic of the optical measurement setup. F, fiber, L, lens. (d)–(f) Calculated R_L, T_L, and $\mathcal{A}_1$ for the full $S + M_1 + Si + M_2 + S$ structure and (g)–(i) the corresponding measurements. The dotted horizontal lines are the theoretical limits for one-sided coherent absorption in a symmetric structure.

(the resonance order m is an integer). The strength of absorption at the resonances is set by the fidelity of the achieved R (for M_1) to the target design [Fig. 2(c)]. In our calculations, we made use of $n(\lambda)$ obtained from ellipsometric measurements. In comparing the measurements and theoretical predictions of R_L, T_L, and $\mathcal{A}_1$ for the symmetric device, we note that the greatest deviation is in the vicinity of $\lambda = 1300$ nm, where the reflectivity of M_1 departs from the target values [Fig. 3(c)]. A similar deviation occurs at the short wavelength edge (~800 nm). In general, reaching the theoretical value of $\mathcal{A}_1 = 0.5$ at any resonance is readily predicted by the proximity of R to the target.

We have carried out one-sided-incidence measurements on the asymmetric device and compared the measured and theoretically predicted values of R_L, T_L, and $\mathcal{A}_1^a$ over a full spectral octave [Fig. 5]. In contrast to $\mathcal{A}_1$ in Fig. 4, $\mathcal{A}_1^a$ is substantially larger than the symmetric device limit of $\mathcal{A}_1 \geq 0.5$. Deviations from achieving the theoretical limit of $\mathcal{A}_1^a$ are associated with inaccuracies in mirror fabrication, which manifest themselves in differences between the target and measured reflectivities. Our measurements in Fig. 3 and statistical simulations indicate that there is ~5% error in the layer thicknesses of the fabricated mirrors. Reducing this error to ~2% makes the resulting deviations in mirror reflectivity have negligible impact on the effective absorption.

A milestone in the development of ultrabroad-bandwidth lasers [26] was the realization that spectrally flat-chirped mirrors [27] enable control over the cavity dispersion via their spectral *phase*. We have shown that the CPA bandwidth is increased through control over the spectral reflectivity *amplitude* of the mirrors in a lossy cavity. By implementing this principle, we have demonstrated CPA over a full octave, ~800–1600 nm that is dramatically broader than previous experimental results. Our results demonstrate that the judicious design of the photonic environment of a lossy material allows one to controllably sever the link between the *effective* optical absorption in the structure and the *intrinsic* absorption of the material from which it is constructed. We have focused here on absorption in Si, but our approach is applicable to any other material that may be processed into a film. The bandwidth is limited only by the fabrication precision, which constrains how precisely R tracks the spectral changes in $\mathcal{A}$. The challenge of extending the CPA effect to *continuously* cover the spectrum can be addressed using the concept of "omni-resonant cavities" in which the wavelength and incidence angles are correlated through the action of a tilted grating [28]. We have thus created the basis for a transformative method that may potentially address a host of critical challenges, including harnessing infrared solar energy, achieving flat spectral sensitivity for photodetectors and maximizing pump absorption in lasers, using only planar technology.

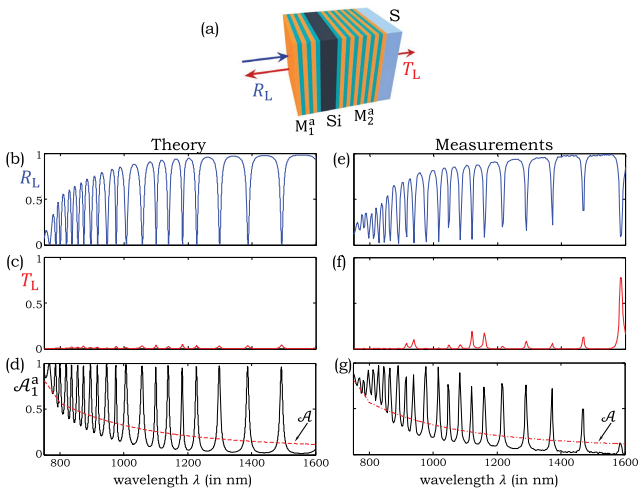

Fig. 5. One-sided CPA in an asymmetric cavity. (a) Schematic of the device; S, substrate. (b)–(d) Theoretical predictions of R_L, T_L, and $\mathcal{A}_1^a$ for the full M_1^a + Si + M_1^a + S structure, and (e)–(g) the corresponding measurements. The dotted lines in (d) and (g) correspond to $\mathcal{A}$ for a 2 μm thick Si film [Fig. 2(b)].

Funding. U.S. Air Force Office of Scientific Research (AFOSR) (FA9550-14-1-0037).

Acknowledgment. The authors thank J. D. Perlstein, S. Teroghi, F. A. Tan, J. J. Kaufman, F. Goldstein, K. George, Sr., K. George, Jr., and M. Chase for technical assistance. The authors also acknowledge useful discussions with D. N. Christodoulides and M. Bayat.

REFERENCES

1. A. Guo, G. J. Salamo, D. Duchesne, R. Morandotti, M. Volatier-Ravat, V. Aimez, G. A. Siviloglou, and D. N. Christodoulides, Phys. Rev. Lett. **103**, 093902 (2009).
2. L. Feng, Y.-L. Xu, W. S. Fegadolli, M.-H. Lu, J. E. B. Oliveira, V. R. Almeida, Y.-F. Chen, and A. Scherer, Nat. Mater. **12**, 108 (2012).
3. C. E. Rüter, K. G. Makris, R. El-Ganainy, D. N. Christodoulides, M. Segev, and D. Kip, Nat. Phys. **6**, 192 (2010).
4. A. Regensburger, C. Bersch, M.-A. Miri, G. Onishchukov, D. N. Christodoulides, and U. Peschel, Nature **488**, 167 (2012).
5. Y. D. Chong, L. Ge, H. Cao, and A. D. Stone, Phys. Rev. Lett. **105**, 053901 (2010).
6. W. Wan, Y. Chong, L. Ge, H. Noh, A. D. Stone, and H. Cao, Science **331**, 889 (2011).
7. Y. D. Chong and A. D. Stone, Phys. Rev. Lett. **107**, 163901 (2011).
8. A. Yariv, Electron. Lett. **36**, 321 (2000).
9. A. Yariv, IEEE Photon. Technol. Lett. **14**, 483 (2002).
10. J. C. Slater, *Microwave Electronics* (D. Van Nostrand, 1950).
11. J. Shi, X. Fang, E. T. F. Rogers, E. Plum, K. F. MacDonald, and N. I. Zheludev, Opt. Express **22**, 21051 (2014).
12. S. A. Mousavi, E. Plum, J. Shi, and N. I. Zheludev, Appl. Phys. Lett. **105**, 011906 (2014).
13. X. Fang, K. F. MacDonald, and N. I. Zheludev, Light Sci. Appl. **4**, e292 (2015).
14. G. Pirruccio, L. M. Moreno, G. Lorenzo, and J. G. Rivas, ACS Nano **7**, 4810 (2013).
15. J. R. Piper and S. Fan, ACS Photon. **1**, 347 (2014).
16. J. Z. Song, P. Bai, Z. H. Hang, and Y. Lai, New J. Phys. **16**, 033026 (2014).
17. Z. Li, S. Zhang, N. J. Halas, P. Nordlander, and H. Xu, Small **7**, 593 (2011).
18. J. W. Yoon, G. M. Koh, S. H. Song, and R. Magnusson, Phys. Rev. Lett. **109**, 257402 (2012).
19. J. Zhang, K. F. MacDonald, and N. I. Zheludev, Light Sci. Appl. **1**, e18 (2012).
20. S. Dutta-Gupta, O. J. F. Martin, S. D. Gupta, and G. S. Agarwal, Opt. Express **20**, 1330 (2012).
21. M. Pu, Q. Feng, M. Wang, C. Hu, C. Huang, X. Ma, Z. Zhao, C. Wang, and X. Luo, Opt. Express **20**, 2246 (2012).
22. M. L. Villinger, M. Bayat, L. N. Pye, and A. F. Abouraddy, Opt. Lett. **40**, 5550 (2015).
23. A. Zeilinger, Am. J. Phys. **49**, 882 (1981).
24. J. Meiron, J. Opt. Soc. Am. **55**, 1105 (1965).
25. D. A. B. Miller, J. Opt. Soc. Am. B **24**, A1 (2007).
26. T. Brabec and F. Krausz, Rev. Mod. Phys. **72**, 545 (2000).
27. R. Szipöcs, K. Ferencz, C. Spielmann, and F. Krausz, Opt. Lett. **19**, 201 (1994).
28. S. Shabahang, H. E. Kondakci, M. L. Villinger, J. D. Perlstein, and A. F. Abouraddy, "Omni-resonant optical micro-cavity," arXiv:1612.04328 (2016).